Multispin Ising spin glasses with ferromagnetic interactions

Peter Gillin[1], Hidetoshi Nishimori[2], and David Sherrington[1]

[1] Physics Department, University of Oxford, Theoretical Physics, 1 Keble Road, Oxford OX1 3NP, UK

[2] Department of Physics, Tokyo Institute of Technology, Oh-Okayama, Meguro-ku, Tokyo 152-8551, Japan

Abstract

We consider the thermodynamics of an infinite-range Ising p-spin glass model with an additional r-spin ferromagnetic interaction. For $r = 2$ there is a continuous transition to a ferromagnetic phase, while for $r > 2$ the transition is first order. We find both glassy and non-glassy ferromagnetic phases, with replica symmetry breaking of both the one step and full varieties. We obtain new results for the case where $r = p > 2$, demonstrating the existence of a non-glassy ferromagnetic phase, of significance to error-correcting codes.

1 Introduction

Competition between quenched randomness, frustration, and a tendency to order uniformly causes non-trivial behaviour in many-body systems. Typical examples include spin glasses with ferromagnetic bias [1–3], neural networks [4], proteins [5], and error-correcting codes [6]. When the quenched randomness dominates, these systems exhibit randomly frozen (spin glass) states. When the ordering tendency dominates, they exhibit uniformly ordered (non-glassy ferromagnetic) states. In the intermediate regime they can exhibit mixed (glassy ferromagnetic) states. The phase diagrams around this crossover often have a rich structure.

One of the principal purposes of this paper is to present a new method to construct the phase diagrams of such systems from an understanding of the related system with only the random term and an external field term. We apply this method to an Ising spin glass with a p-spin Gaussian random interaction and an r-spin ordering interaction, both of infinite range. It has been shown [7] using replica theory that for $p > 2$, the system with neither ordering nor field terms has two phase transitions: a discontinuous one step replica symmetry breaking, followed by a full replica symmetry breaking at lower temperature. Subsequent work investigated the one step transition with the addition of either a field [8] or an ordering interaction with $r = p$ [9]. We extend the results to the case of general r and also examine the transition from one step to full replica symmetry breaking. This work follows on from a previous paper [10] in which we dealt not with an Ising spin system, but with a technically simpler spherical spin system.

The order of the paper is as follows. In §2 we present the general method. In §3 we review the replica theory of the Ising p-spin glass. In §4 we discuss the phase diagrams of the Ising p-spin glass with r-spin ferromagnetism. In §5 we present some exact results using a gauge transformation for the case where $r = p$. Finally, we make concluding remarks and present technical appendices.

2 The constrained magnetization approach to mean field ferromagnetism

We consider a general system of scalar spins with a Hamiltonian

$$\mathcal{H}_r(J_0) = \mathcal{H}_{\text{base}} - \frac{J_0(r-1)!}{N^{r-1}} \sum_{i_1<i_2\cdots<i_r} \sigma_{i_1} \ldots \sigma_{i_r} \tag{1}$$

where the first term is the Hamiltonian of any system (referred to as the base system), and the second term is an infinite-range r-spin ferromagnetic interaction. To leading order in $1/N$ the

partition function is

$$Z_r(J_0) = \sum_{\{\sigma_i\}} \exp\left[-\beta\mathcal{H}_{\rm base} + N\beta J_0 \frac{1}{r}\left(\frac{1}{N}\sum_i \sigma_i\right)^r\right] \tag{2}$$

$$= \int dM\ \exp -N\beta\left(f_{\rm base}(M) - \frac{1}{r}J_0 M^r\right) \tag{3}$$

where

$$f_{\rm base}(M) = -\frac{1}{N\beta}\ln Z_{\rm base}(M)\,, \tag{4}$$

$$Z_{\rm base}(M) = \sum_{\{\sigma_i\}} \delta\left(M - \frac{1}{N}\sum_i \sigma_i\right) \exp -\beta\mathcal{H}_{\rm base}\,. \tag{5}$$

We recognize $f_{\rm base}(M)$ as the free energy per site of the base system when the magnetization per spin is constrained (via the δ-function in the partition function) to be M. Given a knowledge of this function, we can carry out the integral over M in (3) to leading order in $1/N$ by the saddle point method, giving a free energy per spin of

$$f_r(J_0) = -\frac{1}{N\beta}\ln Z_r(J_0) = f_{\rm base}(M_r) - \frac{1}{r}J_0 M_r^r \tag{6}$$

where the equilibrium magnetization $M_r(J_0)$ minimizes the right hand side, and so is a solution to the equation

$$f'_{\rm base}(M_r) = J_0 M_r^{r-1}. \tag{7}$$

We note further that if we take $r = 1$, the second term of (1) represents an external magnetic field $h = J_0$, and so the free energy of the constrained base system is related simply to that of the unconstrained base system in an external magnetic field by

$$f_{\rm field}(h) = f_{\rm base}(M_{\rm field}(h)) - hM_{\rm field}(h), \tag{8}$$

$$f'_{\rm base}(M_{\rm field}(h)) = h\,. \tag{9}$$

Therefore a knowledge of the free energy of either system is enough to determine that of the ferromagnetic system via (6) and (7): the ferromagnetic term acts as an effective field

$$h = J_0 M^{r-1} \tag{10}$$

which must be determined self-consistently.

3 The replica theory of the Ising p-spin glass

In the remainder of this paper we shall concentrate on the example of an infinite-ranged Ising p-spin glass model. The Hamiltonian we use is

$$\mathcal{H}_r = \sum_{i_1<i_2\cdots<i_p} J_{i_1\ldots i_p}\sigma_{i_1}\ldots\sigma_{i_p} - \frac{J_0(r-1)!}{N^{r-1}}\sum_{i_1<i_2\cdots<i_r}\sigma_{i_1}\ldots\sigma_{i_r} \tag{11}$$

where $J_{i_1\ldots i_p}$ are independent quenched random couplings given by a Gaussian distribution with zero mean and variance $p!J^2/2N^{p-1}$, and $\sigma_i = \pm 1$ are Ising spins. For $p = 2$ we recover a generalized Sherrington–Kirkpatrick model [11,12] which has only full replica symmetry breaking. In the present paper we consider $p > 2$ so that there also is a region of one step replica symmetry breaking. In the limit $p \to \infty$, we recover the random energy model (REM) [13, 14] which has no full replica symmetry breaking: this will be discussed further in §4.

In the spirit of the previous section, we consider first the simpler

$$\mathcal{H}_{\rm field} = \sum_{i_1<i_2\cdots<i_p} J_{i_1\ldots i_p}\sigma_{i_1}\ldots\sigma_{i_p} - h\sum_i \sigma_i\,. \tag{12}$$

Previous studies [7–9] used the replica method [1, 2] to obtain the free energy per site $f_{\rm field}$ given by

$$\beta f_{\rm field} = \lim_{n\to 0}\frac{1}{n}\left[\frac{1}{4}(p-1)\beta^2J^2\sum_{a\neq b}q_{ab}^p - \ln\sum_{\{\sigma^a\}}\exp\left(\frac{1}{4}p\beta^2J^2\sum_{a\neq b}q_{ab}^{p-1}\sigma^a\sigma^b + \beta h\sum_a\sigma^a\right)\right] - \frac{\beta^2J^2}{4} \tag{13}$$

which must be extremized for the replica overlaps $q_{ab} = \frac{1}{N}\sum_i\langle\sigma_i^a\sigma_i^b\rangle$ for $1\leqslant a\neq b\leqslant n$. In the replica symmetric (RS) ansatz ($q_{ab}=q$ for all $a\neq b$) this is

$$\beta f_{\rm field}^{\rm (RS)} = -\frac{1}{4}(p-1)\beta^2J^2q^p - \frac{1}{4}\beta^2J^2 + \frac{1}{4}p\beta^2J^2q^{p-1} - \int\frac{dz}{\sqrt{2\pi}}\,e^{-z^2/2}\ln 2\cosh\left(\sqrt{\tfrac{1}{2}p\beta^2J^2q^{p-1}}\,z+\beta h\right) \tag{14}$$

where the overlap q is given by the self-consistency equation

$$q = \int\frac{dz}{\sqrt{2\pi}}\,e^{-z^2/2}\tanh^2\left(\sqrt{\tfrac{1}{2}p\beta^2J^2q^{p-1}}\,z+\beta h\right). \tag{15}$$

This RS solution is stable against small replica symmetry breaking Almeida–Thouless fluctuations [15] if

$$\frac{1}{2}p(p-1)\beta^2J^2q^{p-2}\int\frac{dz}{\sqrt{2\pi}}\,e^{-z^2/2}\,\mathrm{sech}^4\left(\sqrt{\tfrac{1}{2}p\beta^2J^2q^{p-1}}\,z+\beta h\right) < 1\,. \tag{16}$$

The magnetization of the RS solution is

$$M = \int\frac{dz}{\sqrt{2\pi}}\,e^{-z^2/2}\tanh\left(\sqrt{\tfrac{1}{2}p\beta^2J^2q^{p-1}}\,z+\beta h\right). \tag{17}$$

In the one step replica symmetry breaking (1RSB) ansatz [16] the free energy per site is $f_{\rm field}^{\rm (1RSB)}$ given by

$$\beta f_{\rm field}^{\rm (1RSB)} = -\frac{1}{4}(p-1)\beta^2J^2\left[(1-x)q_1^p + xq_0^p\right] - \frac{1}{4}\beta^2J^2 + \frac{1}{4}p\beta^2J^2q_1^{p-1} - \frac{1}{x}\int\frac{dz_0}{\sqrt{2\pi}}\,e^{-z_0^2/2}\ln 2^x\int\frac{dz_1}{\sqrt{2\pi}}\,e^{-z_1^2/2}\cosh^x G \tag{18}$$

where

$$G \doteq \sqrt{\tfrac{1}{2}p\beta^2J^2q_0^{p-1}}\,z_0 + \sqrt{\tfrac{1}{2}p\beta^2J^2(q_1^{p-1}-q_0^{p-1})}\,z_1 + \beta h\,, \tag{19}$$

and the mutual overlap q_0, the self overlap q_1, and the break point x (i.e. the weight of q_0 in the averaged overlap distribution function) are given by the self-consistency equations

$$q_0 = \int\frac{dz_0}{\sqrt{2\pi}}\,e^{-z_0^2/2}\left(\frac{\int\frac{dz_1}{\sqrt{2\pi}}\,e^{-z_1^2/2}\cosh^x G\,\tanh G}{\int\frac{dz_1}{\sqrt{2\pi}}\,e^{-z_1^2/2}\cosh^x G}\right)^2, \tag{20a}$$

$$q_1 = \int\frac{dz_0}{\sqrt{2\pi}}\,e^{-z_0^2/2}\,\frac{\int\frac{dz_1}{\sqrt{2\pi}}\,e^{-z_1^2/2}\cosh^x G\,\tanh^2 G}{\int\frac{dz_1}{\sqrt{2\pi}}\,e^{-z_1^2/2}\cosh^x G}, \tag{20b}$$

$$\frac{1}{4}(p-1)\beta^2J^2(q_1^p-q_0^p) = -\frac{1}{x^2}\int\frac{dz_0}{\sqrt{2\pi}}\,e^{-z_0^2/2}\,\ln\int\frac{dz_1}{\sqrt{2\pi}}\,e^{-z_1^2/2}\cosh^x G + \frac{1}{x}\int\frac{dz_0}{\sqrt{2\pi}}\,e^{-z_0^2/2}\,\frac{\int\frac{dz_1}{\sqrt{2\pi}}\,e^{-z_1^2/2}\cosh^x G\,\ln\cosh G}{\int\frac{dz_1}{\sqrt{2\pi}}\,e^{-z_1^2/2}\cosh^x G}. \tag{20c}$$

This 1RSB solution is stable against further replica symmetry breaking fluctuations if

$$\frac{1}{2}p(p-1)\beta^2 J^2 q_1^{p-2} \int \frac{dz_0}{\sqrt{2\pi}}\, e^{-z_0^2/2}\, \frac{\int \frac{dz_1}{\sqrt{2\pi}}\, e^{-z_1^2/2} \cosh^{x-4} G}{\int \frac{dz_1}{\sqrt{2\pi}}\, e^{-z_1^2/2} \cosh^{x} G} < 1\,. \tag{21}$$

Where the 1RSB solution becomes unstable, we expect a continuous transition to a solution given by the full Parisi ansatz, which we do not consider in detail here. The magnetization of the 1RSB solution is

$$M = \int \frac{dz_0}{\sqrt{2\pi}}\, e^{-z_0^2/2}\, \frac{\int \frac{dz_1}{\sqrt{2\pi}}\, e^{-z_1^2/2} \cosh^{x} G \tanh G}{\int \frac{dz_1}{\sqrt{2\pi}}\, e^{-z_1^2/2} \cosh^{x} G}. \tag{22}$$

4 Full results and phase diagrams

The phase diagrams for the Hamiltonian (11) were found in two stages. They are shown for $p = 5$ and $r = 1, \ldots, 6$ in figure 1.

Firstly, the free energy and magnetization of the system in a field but without ferromagnetism, as given by (12), were found. The RS solution was found by numerical solution of (15), the 1RSB by numerical solution of (20). No attempt was made to determine the solution with full replica symmetry breaking (FRSB) in the Parisi scheme, but the onset of unstable modes in the 1RSB solution, as given by (21), is taken to signify a continuous transition to FRSB.

The resulting phase diagram for $p = 5$ is plotted in figure 1(a). This Hamiltonian is equivalent to (11) with $p = 5$, $r = 1$, and $J_0 = h$. There are three phases: an RS paramagnet, a 1RSB spin glass, and an FRSB spin glass. The replica symmetry breaking transition curve has been found previously [8]. Where the field is less than a critical value, there is a discontinuous one step RSB transition (D1RSB) where $x = 1$, and the transition temperature rises with h. Above the critical value, the transition is continuous, first continuous one step (C1RSB) where $q_0 = q_1$, and then FRSB; and the transition temperature falls with h, vanishing asymptotically as $h \to \infty$. (Note that the D1RSB transition is continuous in the thermodynamic sense.) The numerical calculation of the 1RSB/FRSB curve is troublesome near the C1RSB transition line: this is because the difference between the left and right hand sides of (21) is very small, of the order of $(q_1 - q_0)^4$. Consequently we do not have reliable results in this region, and a small gap is left in the plot to indicate this. However, the point where this curve meets the C1RSB line (which we shall call the RSB triple point, since RS, 1RSB, and FRSB phases meet at it) has been determined accurately using the RS solution and a perturbative calculation, details of which are given in Appendix A. The magnetization M was calculated with (17) and (22), and curves of h as a function of M at fixed temperature for $p = 5$ are shown in figure 2. We indicate where the solution is of each type (RS, 1RSB, FRSB), but note that h is not exact in the FRSB region, since it is approximated by the 1RSB value.

Secondly, the methods of §2 were used to calculate the transitions in the full Hamiltonian, essentially by finding the stable solutions of (10) with the $h(M)$ found previously. (In the FRSB region, the use of the 1RSB values introduces a small error in the ferromagnetic transition lines.) The resulting phase diagrams for $p = 5$ and $r = 2, \ldots, 6$ are plotted in figures 1(b)–1(f).

For $r = 2$ and $p > 2$, the phase diagram contains six regions. For small J_0, there are three $M = 0$ phases: on cooling, the RS paramagnet undergoes first a D1RSB transition, and then an FRSB (not shown explicitly in figure 1). Increasing J_0, the $M = 0$ phases become unstable, and a continuous transition to $M \neq 0$ occurs. There are three ferromagnetic phases: RS, 1RSB, and FRSB. Within the ferromagnetic region, the RS/1RSB curve has D1RSB and C1RSB parts, as for $r = 1$. (The RS/1RSB transition in the $M = 0$ region is always D1RSB, since the effective field $J_0 M^{r-1}$ vanishes.)

For $r > 2$, the ferromagnetic transition is first order: on increasing J_0, there is first a spinodal transition, at which a metastable $M \neq 0$ solution appears, followed by a thermodynamic transition, at which the comparative free energies make it the favoured state.

Increasing r at fixed p, we identify two qualitative changes, illustrated in figure 3. For r slightly greater than 2, the diagram has the form of figure 3(a). On increasing r, the peak of

p	3	4	5	6	8	10
r_1	2.92	3.82	4.72	5.62	7.44	9.30
r_2	3.01	3.98	4.95	5.91	7.83	9.76

Table 1: Special values of r for various choices of p. There is no D1RSB curve in the ferromagnet for $r \geqslant r_1$, and no 1RSB region in the ferromagnet for $r \geqslant r_2$.

the RS/1RSB curve approaches the spinodal ferromagnetic transition line, and the D1RSB curve between them shortens. The peak reaches the spinodal line for $r = r_1$, and there is no D1RSB curve in the ferromagnetic region for $r \geqslant r_1$, as in figure 3(b). The RSB triple point approaches the spinodal ferromagnetic transition line on increasing r, and the 1RSB region shrinks. The triple point reaches the spinodal line at $r = r_2$, and there is no ferromagnetic 1RSB region for $r \geqslant r_2$, as in figure 3(c). These special values of r may be evaluated for given p with some accuracy, as discussed in Appendix B. Some results are shown in table 1. They are in accordance with an exact result, to be proved in §5, that r_1 cannot exceed p.

Of particular interest is the behaviour of the model in the case $r = p$; this is relevant to error-correcting codes [6], and is amenable to an exact calculation on the Nishimori line. We observe that there is a first order transition to a ferromagnetism which is glassy for small enough values of J_0 and T, and that there is a triple point where the spinodal ferromagnetic transition line and the glassy transition line within the ferromagnet meet with infinite slope. (Exact results in the $r = p$ case, including the fact that the solution is RS on the line $p\beta J^2 = 2J_0$, are given in §5.) The RSB region shrinks as $r = p$ increases. The existence of an RS ferromagnetic phase persists in the limit $r = p \to \infty$. Our results therefore contradict conclusions of Dorlas and Wedagedera [14], who claim that the ferromagnetic region in the model with $r = p \to \infty$ is entirely glassy. This discrepancy is due to the order in which the limits $r \to p$ and $p \to \infty$ are taken. The approach of Dorlas and Wedagedera is to consider the REM with general r, effectively taking the limit $p \to \infty$ in the Ising model, and to subsequently take the limit $r \to \infty$. In doing this, they obtain results which would apply to $p \gg r \to \infty$. In our approach we set $r = p$ and then take $p \to \infty$, obtaining results which apply to $r = p \to \infty$, the appropriate case when one considers error-correcting codes [6]. This difference may be illustrated using figures 1(c) and 1(e): the former is for $r < p$, and the ferromagnetic phase is dominated by the 1RSB region in the limit $p \to \infty$ with $r < p$; the latter is for $r = p$, and the ferromagnetic phase is dominated by the RS region in the limit $r = p \to \infty$.

5 Special features on the Nishimori line

Some of our conclusions about the phase diagram for $r = p$ are reinforced from a different point of view. We show in the present section that on the Nishimori line, the distribution function of the spin glass order parameter consists only of two delta functions. This immediately implies that the ferromagnetic phase is not glassy on the Nishimori line for any $r = p$.

We start our argument from the definition of the distribution function of magnetization under the Hamiltonian (11) with $r = p$:

$$P_m(y) = \left[\frac{\sum_{\{\sigma_i\}} \delta(y - N^{-1} \sum_i \sigma_i) \exp\left(-\beta \mathcal{H}_p\right)}{\sum_{\{\sigma_i\}} \exp\left(-\beta \mathcal{H}_p\right)} \right]_J . \tag{23}$$

Here the outer brackets denote the configurational average over the Gaussian distribution of exchange interactions. To define the distribution function of the spin glass order parameter, it is convenient to introduce two replicas of the same system, with spins $\{\sigma_i^{(1)}\}$ and $\{\sigma_i^{(2)}\}$:

$$P_q(y) = \left[\frac{\sum_{\{\sigma_i^{(1)}\}} \sum_{\{\sigma_i^{(2)}\}} \delta(y - N^{-1} \sum_i \sigma_i^{(1)} \sigma_i^{(2)}) \exp\left(-\beta \mathcal{H}_p(\{\sigma_i^{(1)}\}) - \beta \mathcal{H}_p(\{\sigma_i^{(2)}\})\right)}{\sum_{\{\sigma_i^{(1)}\}} \sum_{\{\sigma_i^{(1)}\}} \exp\left(-\beta \mathcal{H}_p(\{\sigma_i^{(1)}\}) - \beta \mathcal{H}_p(\{\sigma_i^{(2)}\})\right)} \right]_J . \tag{24}$$

Our main result is the identity

$$P_m(y) = P_q(y) \qquad \text{wherever} \qquad p\beta J^2 = 2J_0. \tag{25}$$

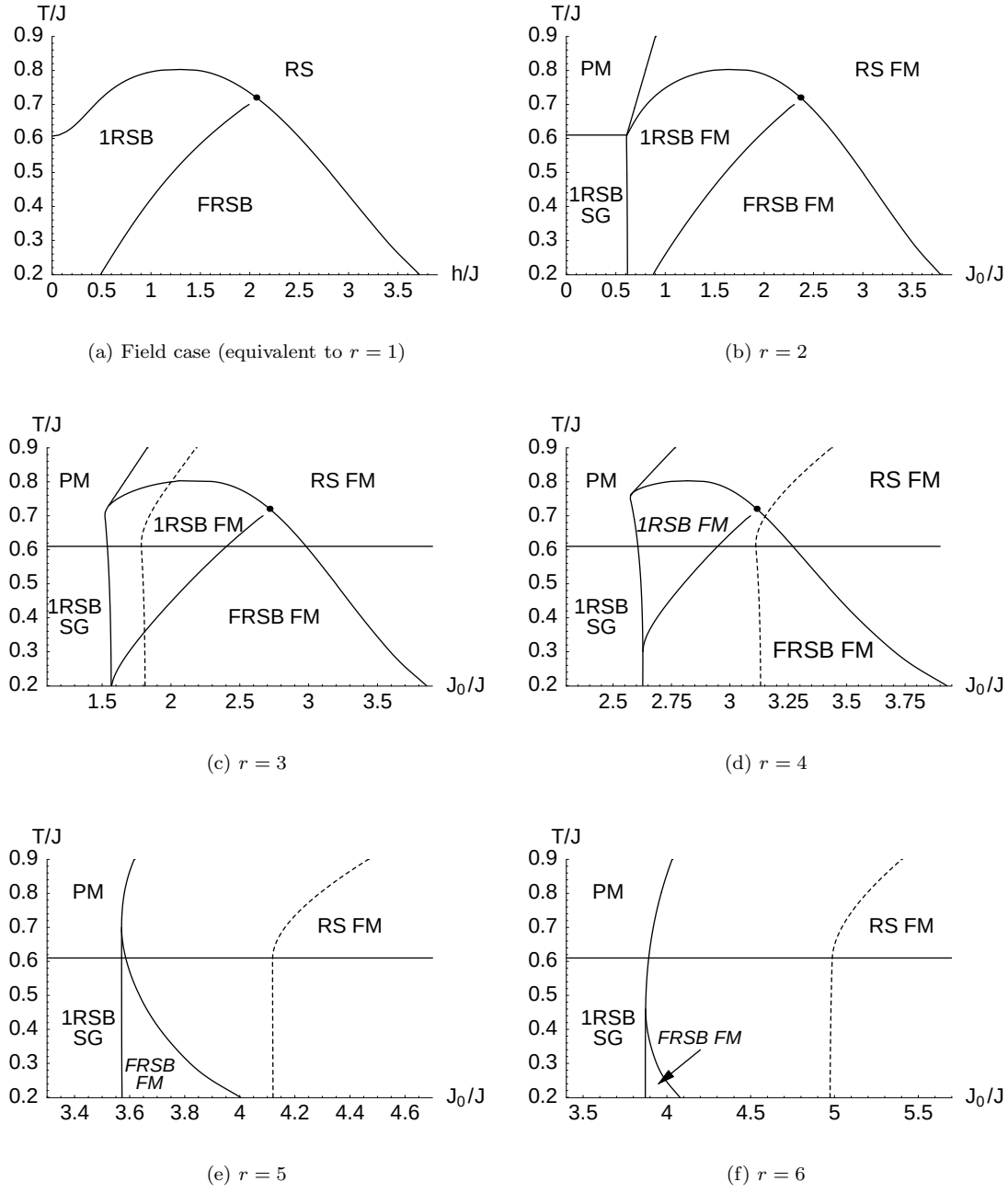

(a) Field case (equivalent to $r = 1$)

(b) $r = 2$

(c) $r = 3$

(d) $r = 4$

(e) $r = 5$

(f) $r = 6$

Figure 1: The phase diagrams calculated in §4 for the systems given by (a) the Hamiltonian (12) with $p = 5$, and (b)–(f) the Hamiltonian (11) with $p = 5$ and $r = 2, \ldots, 6$. The phases are labelled by their symmetry breaking (RS, 1RSB, and FRSB) and, for $r \geqslant 2$, by their ferromagnetism ($M = 0$ for the paramagnetic (PM) and spin glass (SG) phases, while $M \neq 0$ for the ferromagnetic (FM) phases). For $r > 2$, where the ferromagnetic transition is first order, the spinodal transition is shown with a solid line, and the thermodynamic transition with a dashed line; phases labelled in italics are metastable. The RSB triple point (found by the perturbative calculation of Appendix A) is shown as a circle. (The transition to FRSB is at a temperature too low to appear for small h or J_0, in particular within the spin glass phase where the effective field vanishes.)

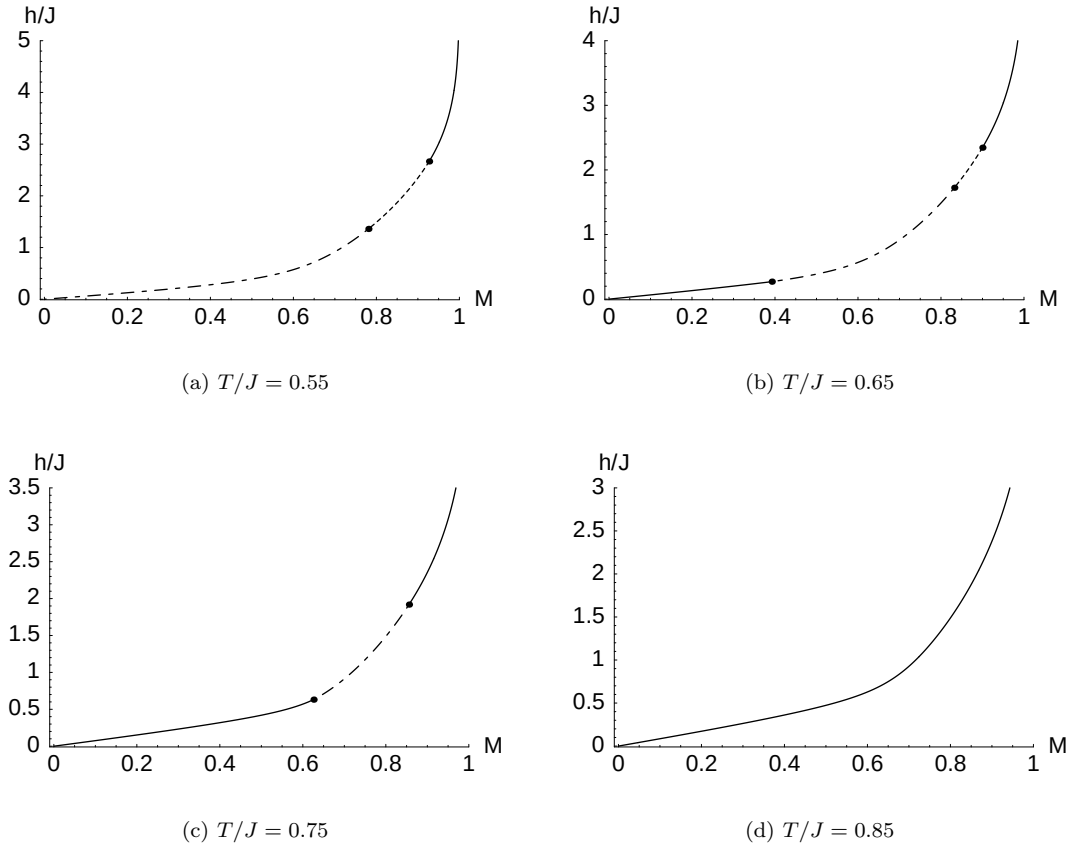

(a) $T/J = 0.55$

(b) $T/J = 0.65$

(c) $T/J = 0.75$

(d) $T/J = 0.85$

Figure 2: The field h as a function of the magnetization M for the system given by the Hamiltonian (12) with $p = 5$, as calculated in §4, at various temperatures. The solid curves show RS solutions, the dot-dashed curves 1RSB, and the dashed curves FRSB; the points mark the transitions. The field here is identical to the effective field $J_0 M^{r-1}$ in the system with Hamiltonian (11), as discussed in §2.

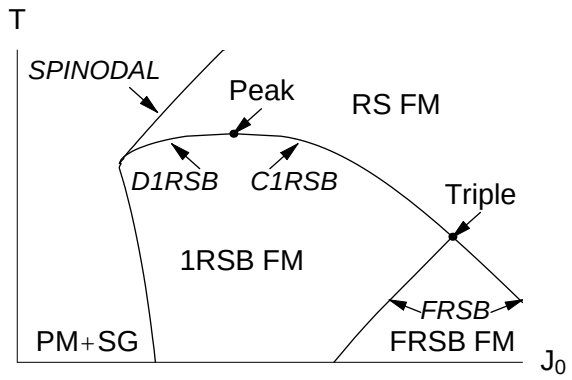

(a) $r < r_1$

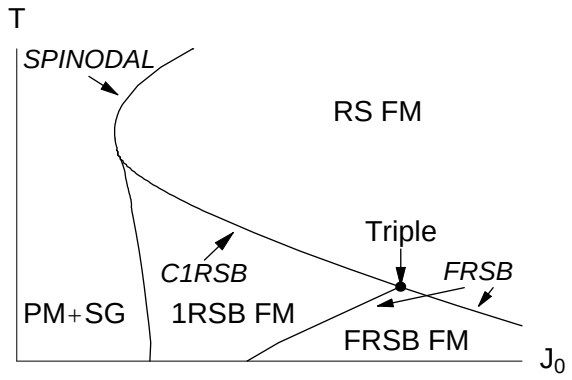

(b) $r_1 < r < r_2$

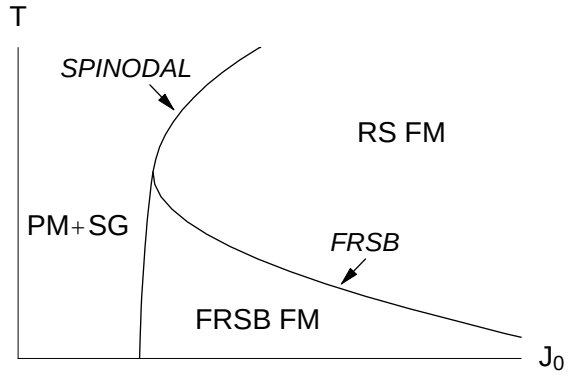

(c) $r > r_2$

Figure 3: Phase diagrams for the system given by the Hamiltonian (11), illustrating the qualitative changes on increasing r at fixed p. The ferromagnetic phases are labelled according to their replica symmetry breaking. For clarity, the paramagnetic and spin glass phases are amalgamated and the RSB transitions in the $M = 0$ solution are not shown. The spinodal transition and the RSB transitions in the ferromagnetic phase are labelled in italics. The peak in the RS AT line and the RSB triple point are also labelled where present. On increasing r, both these points move towards the spinodal line.

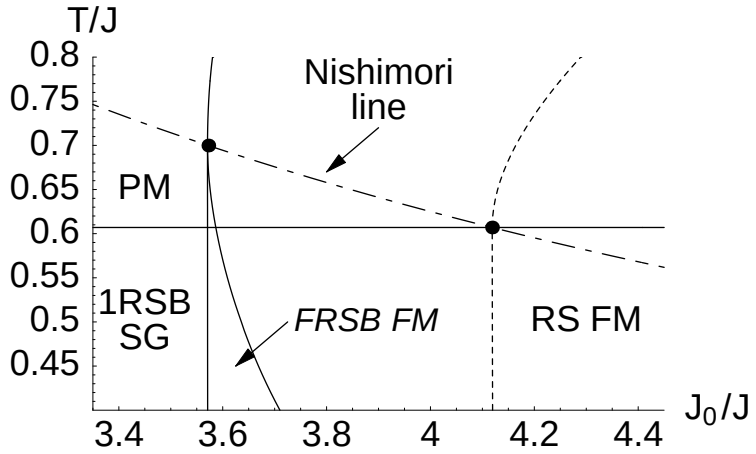

Figure 4: A section of the phase diagram for the system given by the Hamiltonian (11) with $r = p = 5$, as figure 1(e), showing the Nishimori line $p\beta J^2 = 2J_0$ as a dot-dashed line. The solution is replica symmetric with $M = q$ on this curve, as discussed in §5. The lower-right point marks where the paramagnetic, spin glass, and RS ferromagnetic phases meet in thermodynamics. The upper-left point marks where the paramagnetic, the RS ferromagnetic, and the FRSB ferromagnetic phases meet in spinodals. The Nishimori line passes through both points.

The condition $p\beta J^2 = 2J_0$ defines a curve in the phase diagram called the Nishimori line [17]. This line passes through the paramagnetic and ferromagnetic phases as shown by the dot-dashed curve in figure 4. The result is proved in Appendix C.1.

It is well established that the distribution of magnetization $P_m(y)$ has a simple structure with two delta functions at symmetric positions. Then (25) proves that the distribution function of the spin glass order parameter $P_q(y)$ is also simple on the Nishimori line, which is not the case if the ferromagnetic phase is glassy.

In Appendix C.2 we demonstrate three further facts about the Nishimori line: it passes through the point where the spin glass transition line meets the thermodynamic ferromagnetic transition line (the lower-right point marked in figure 4); at this point, the q_1 of the spin glass and the q of the ferromagnet are equal; and it passes through the point where the continuous glassy transition line (or, equivalently, the RS Almeida–Thouless line) within the ferromagnetic phase meets the spinodal ferromagnetic transition line (the upper-left point marked in figure 4). This last result demonstrates that there is no D1RSB transition line within the ferromagnetic region at $r = p$, as the continuous glassy transition reaches the spinodal line which marks the edge of the ferromagnetic phases. It follows that $r_1 \leqslant p$, as claimed in §4.

6 Conclusions

In this paper, we have shown that the behaviour of a spin glass with an r-spin ferromagnetic interaction of infinite range is simple to obtain from a knowledge of the free energy either of the base spin glass with a constrained magnetization, or equivalently of the base spin glass in an external field (although these latter problems are often numerically subtle); and we have applied this method to an Ising glass with a p-spin Gaussian random interaction. We have found that, for $p > 2$ and $r \geqslant 2$, there are both glassy and non-glassy ferromagnetic phases; and that for r less than a p-dependent critical value the glassy ferromagnet has regions of both one step and full replica symmetry breaking, while for higher r it has only full replica symmetry breaking. We have also proved several exact results for the case where $r = p$, which is relevant to error-correcting codes: in particular, we have explicitly shown the existence of a curve of simple form in the phase diagram, passing through both paramagnetic and ferromagnetic phases, on which the solution is certainly non-glassy. We hope that the present analysis will stimulate investigation of the phase

structures of related systems.

Appendix A Results from perturbation theory close to the Almeida–Thouless line

In this appendix we derive expression for $x_{\rm c}$, the value of x along the C1RSB curve, and the condition to determine the RSB triple point where the RS, 1RSB, and FRSB ferromagnetic phases meet. We use the definitions

$$\mathcal{T}_n \doteq \int \frac{dz_0}{\sqrt{2\pi}}\, e^{-z_0^2/2} \tanh^n\left(\sqrt{\tfrac{1}{2}p\beta^2J^2q_0^{p-1}}z_0 + \beta h\right), \tag{26}$$

$$\mathcal{S}_n \doteq \int \frac{dz_0}{\sqrt{2\pi}}\, e^{-z_0^2/2} \operatorname{sech}^n\left(\sqrt{\tfrac{1}{2}p\beta^2J^2q_0^{p-1}}z_0 + \beta h\right). \tag{27}$$

A continuous one step replica symmetry breaking (C1RSB) transition occurs on the line where $q_0 = q_1$ in the 1RSB ansatz. Details of the 1RSB solution close to this line, using only the numerical solution to the RS equation, are obtained by an expansion of these equations in small $\epsilon \doteq (q_1 - q_0)$. Since the hyperbolic functions of G become polynomials in z_1, the integrals over z_1 can be carried out immediately, simplifying matters considerably. In particular, one can find the RSB triple point using only the numerical RS data.

To leading order, both (20a) and (20b) are

$$q_0 = \mathcal{T}_2 + O(\epsilon) \tag{28}$$

and so $q_0 = q + O(\epsilon)$ where q is the RS order parameter satisfying (15). To obtain a second piece of information from these two equations, [(20b) − (20a)] must be expanded to first order, giving

$$\epsilon = \tfrac{1}{2}p(p-1)\beta^2J^2q_0^{p-2}\mathcal{S}_4\,\epsilon + O(\epsilon)^2. \tag{29}$$

This shows that (16) holds as an equality to leading order in ϵ, and hence that the C1RSB transition and the onset of RS AT instability coincide. This is to be expected: where the replica symmetry breaking mode of the RS solution softens, a continuous transition to an RSB solution occurs.

(20c) is trivially satisfied for $q_0 = q_1$. Expanding to first order gives (28) multiplied by $k_1 \doteq \frac{1}{4}p(p-1)\beta^2J^2q_0^{p-2}\epsilon$, which gives no new information. Expanding $[(20c) - k_1(20a)]$ to second order gives (28) multiplied by $k_2 \doteq \frac{1}{8}p(p-1)(p-2)\beta^2J^2q_0^{p-3}\epsilon^2$ plus (29) multiplied by $\frac{1}{2}k_1$, which again gives no new information. Expanding $[(20c) - (k_1+k_2)(20a) - \frac{1}{2}k_1((20b) - (20a))]$ to third order gives

$$\tfrac{1}{12}\left[\tfrac{1}{2}p(p-1)\beta^2J^2q_0^{p-2}\right]^3\mathcal{S}_6(x - x_{\rm c})\epsilon^3 + O(\epsilon)^4 = 0 \tag{30}$$

$$\Rightarrow \qquad x = x_{\rm c} + O(\epsilon) \tag{31}$$

where

$$x_{\rm c} \doteq \frac{2(p-2)q_0^3 + 4p(p-1)\beta^2J^2q_0^{p+2} - 2[p(p-1)\beta^2J^2q_0^p]^2\mathcal{S}_6}{[p(p-1)\beta^2J^2q_0^p]^2\mathcal{S}_6}. \tag{32}$$

This gives a perturbative expression for x on the C1RSB line using only the RS value of q.[1]

The calculation of the 1RSB stability of the C1RSB transition line follows a similar method. Expanding (21) in powers of ϵ, everything up to third order vanishes by the self-consistent equations. Taking a linear combination of the inequality (21) and the equations (20) such that all terms to third order cancel, the fourth order term gives

$$\begin{aligned} &4(p-2)(8p-15)q + 48p(p-1)(p-2)\beta^2J^2q^p \\ &\qquad - 4p^2(p-1)^2\beta^4J^4q^{2(p-1)}\left[4q + 3(p-2)(2+x_{\rm c})\mathcal{S}_6\right] \\ &\qquad\quad + 3p^3(p-1)^3\beta^6J^6q^{3(p-1)}\left[8(1+x_{\rm c})\mathcal{S}_6 - (6+8x_{\rm c}+x_{\rm c}^2)\mathcal{S}_8\right] > 0\,. \end{aligned} \tag{33}$$

[1] Our (32) for $x_{\rm c}$ differs from that given by (36) of de Oliveira and Fontanari [8], due to their omission of one of these higher order corrections. Further details may be found in our comment on that paper [18].

At high temperatures, this is satisfied and the continuous replica symmetry breaking transition is to 1RSB. Below a point (called the RSB triple point) found by solving (15), and (16) and (33) as equalities, the transition is to FRSB. Within the RSB phase there is a line marking a transition between 1RSB and FRSB which meets the RS AT line at this triple point.

Appendix B An equation for the spinodal transition line

In this appendix we use the definition

$$t \doteq \tanh\left(\sqrt{\tfrac{1}{2}p\beta^2J^2q^{p-1}}z + \beta h\right). \tag{34}$$

The spinodal transition to ferromagnetism occurs at the minimum J_0 for which an $M \neq 0$ solution is possible. In the RS region, the ferromagnetic solution is given by (15), (17), and (10). Differentiating these three with respect to h, and using integration by parts,

$$\frac{\partial q}{\partial h} = \int \frac{dz}{\sqrt{2\pi}}\, e^{-z^2/2}\left[(1-3t^2)(1-t^2)\tfrac{1}{2}p(p-1)\beta^2J^2q^{p-2}\frac{\partial q}{\partial h} + 2t(1-t^2)\beta\right], \tag{35}$$

$$\frac{\partial M}{\partial h} = \int \frac{dz}{\sqrt{2\pi}}\, e^{-z^2/2}\left[-t(1-t^2)\tfrac{1}{2}p(p-1)\beta^2J^2q^{p-2}\frac{\partial q}{\partial h} + (1-t^2)\beta\right], \tag{36}$$

$$1 = \frac{\partial J_0}{\partial h}M^{r-1} + (r-1)J_0M^{r-2}\frac{\partial M}{\partial h}. \tag{37}$$

Asserting the spinodal condition $\partial J_0/\partial h = 0$ and eliminating the unwanted derivatives gives

$$M = (r-1)\beta h\left[1 - \int \frac{dz}{\sqrt{2\pi}}\, e^{-z^2/2}\, t^2 - \frac{2\left[\int \frac{dz}{\sqrt{2\pi}}\, e^{-z^2/2}\, t(1-t^2)\right]^2}{\frac{2}{p(p-1)\beta^2J^2q^{p-2}} - \int \frac{dz}{\sqrt{2\pi}}\, e^{-z^2/2}\,(1-t^2)(1-3t^2)}\right]. \tag{38}$$

We are often interested in the intersection between the spinodal line and the C1RSB line. At this point, (16) holds as an equality, and (38) simplifies to

$$M = (r-1)\beta h\left[1 - \int \frac{dz}{\sqrt{2\pi}}\, e^{-z^2/2}\, t^2 - \frac{\left[\int \frac{dz}{\sqrt{2\pi}}\, e^{-z^2/2}\, t(1-t^2)\right]^2}{\frac{dz}{\sqrt{2\pi}}\, e^{-z^2/2}\, t^2(1-t^2)}\right]. \tag{39}$$

This result can be used as discussed in §4. The peak of the 1RSB transition in the ferromagnetic region is given by the solution of the RS self-consistency equation (15), the RS AT condition (16) as an equality, and the D1RSB equation $x_c = 1$ with x_c given by (32). When this peak hits the spinodal line, the D1RSB curve in the ferromagnetic region vanishes. This occurs at $r = r_1$, obtained for given p by solving these three equations and (39). Similarly, the RSB triple point is given by (15), (16) as an equality, and the perturbative 1RSB AT condition (33) as an equality. When this point hits the spinodal line, the 1RSB ferromagnetic region vanishes. This occurs at $r = r_2$, obtained by solving these three equations and (39). Some values are shown in table 1.

Appendix C Proofs for §5

Appendix C.1 Proof from gauge transformation

In this subsection, we prove (25) using a gauge transformation technique. We explicitly write the configurational average appearing in (23):

$$P_m(y) = \int \prod_{i_1<\ldots i_p} P_J(J_{i_1\ldots i_p}) dJ_{i_1\ldots i_p} \frac{1}{Z_J(\beta)} \sum_{\{\sigma_i\}} \delta\left(y - N^{-1}\sum_i \sigma_i\right) \exp\left(-\beta \mathcal{H}_p(\{\sigma_i\})\right) \tag{40}$$

$$\begin{aligned} &= \int \mathcal{D}J \, \exp\left(-\frac{N^{p-1}}{p!J^2} \sum_{i_1<\ldots i_p} J^2_{i_1\ldots i_p}\right) \\ &\quad \times \frac{1}{Z_J(\beta)} \sum_{\{\sigma_i\}} \delta\left(y - \tfrac{1}{N}\sum_i \sigma_i\right) \exp\left[-\beta \sum_{i_1<\ldots i_p} \left(J_{i_1\ldots i_p} - \frac{J_0(p-1)!}{N^{p-1}}\right) \sigma_{i_1}\ldots\sigma_{i_p}\right] \\ &\quad \times \frac{1}{Z_J(\beta)} \sum_{\{\tau_i\}} \exp\left[-\beta \sum_{i_1<\ldots i_p} \left(J_{i_1\ldots i_p} - \frac{J_0(p-1)!}{N^{p-1}}\right) \tau_{i_1}\ldots\tau_{i_p}\right] \end{aligned} \tag{41}$$

where we have introduced a factor of unity at the end, defined $\mathcal{D}J \doteq \prod_{i_1<\ldots i_p} \sqrt{\frac{N^{p-1}}{\pi p J^2}} dJ_{i_1\ldots i_p}$, and $Z_J(\beta)$ is the partition function for a given choice of the couplings $J_{i_1\ldots i_p}$:

$$Z_J(\beta) = \sum_{\{\sigma_i\}} \exp\left[-\beta \sum_{i_1<\ldots i_p} \left(J_{i_1\ldots i_p} - \frac{J_0(p-1)!}{N^{p-1}}\right) \sigma_{i_1}\ldots\sigma_{i_p}\right]. \tag{42}$$

Shifting the integration variable by $J_0(p-1)!/N^{p-1}$ and reordering trivially, we obtain

$$\begin{aligned} P_m(y) = \sum_{\{\tau_i\}} \int \mathcal{D}J \, &\exp\left(-\frac{N^{p-1}}{p!J^2} \sum_{i_1<\ldots i_p} J^2_{i_1\ldots i_p} - \sum_{i_1<\ldots i_p} \frac{2J_0}{pJ^2} J_{i_1\ldots i_p} - \sum_{i_1<\ldots i_p} \frac{J_0^2(p-1)!}{pN^{p-1}J^2}\right) \\ &\times \frac{1}{Z_J(\beta)^2} \sum_{\{\sigma_i\}} \delta\left(y - \tfrac{1}{N}\sum_i \sigma_i\right) \exp\left[-\beta \sum_{i_1<\ldots i_p} J_{i_1\ldots i_p}\sigma_{i_1}\ldots\sigma_{i_p}\right] \\ &\times \exp\left[-\beta \sum_{i_1<\ldots i_p} J_{i_1\ldots i_p}\tau_{i_1}\ldots\tau_{i_p}\right]. \end{aligned} \tag{43}$$

We now perform a gauge transformation with $\sigma_i \to \sigma_i\tau_i$ and $J_{i_1\ldots i_p} \to J_{i_1\ldots i_p}\tau_{i_1}\ldots\tau_{i_p}$, and obtain

$$\begin{aligned} P_m(y) = \sum_{\{\tau_i\}} \int \mathcal{D}J \, &\exp\left(-\frac{N^{p-1}}{p!J^2} \sum_{i_1<\ldots i_p} J^2_{i_1\ldots i_p} - \sum_{i_1<\ldots i_p} \frac{2J_0}{pJ^2} J_{i_1\ldots i_p}\tau_{i_1}\ldots\tau_{i_p} - \sum_{i_1<\ldots i_p} \frac{J_0^2(p-1)!}{pN^{p-1}J^2}\right) \\ &\times \frac{1}{Z_J(\beta)^2} \sum_{\{\sigma_i\}} \delta\left(y - \tfrac{1}{N}\sum_i \sigma_i\tau_i\right) \exp\left[-\beta \sum_{i_1<\ldots i_p} J_{i_1\ldots i_p}\sigma_{i_1}\ldots\sigma_{i_p}\right] \\ &\times \exp\left[-\beta \sum_{i_1<\ldots i_p} J_{i_1\ldots i_p}\right]. \end{aligned} \tag{44}$$

If $2J_0/pJ^2 = \beta$ then exchanging two terms gives

$$P_m(y) = \sum_{\{\tau_i\}} \int \mathcal{D}J \, \exp\left(-\frac{N^{p-1}}{p!J^2} \sum_{i_1<\ldots i_p} J_{i_1\ldots i_p}^2 - \sum_{i_1<\ldots i_p} \frac{2J_0}{pJ^2} J_{i_1\ldots i_p} - \sum_{i_1<\ldots i_p} \frac{J_0^2(p-1)!}{pN^{p-1}J^2} \right)$$
$$\times \frac{1}{Z_J(\beta)^2} \sum_{\{\sigma_i\}} \delta\left(y - \tfrac{1}{N}\sum_i \sigma_i\tau_i \right) \exp\left[-\beta \sum_{i_1<\ldots i_p} J_{i_1\ldots i_p}\sigma_{i_1}\ldots\sigma_{i_p} \right]$$
$$\times \exp\left[-\beta \sum_{i_1<\ldots i_p} J_{i_1\ldots i_p}\tau_{i_1}\ldots\tau_{i_p} \right] . \tag{45}$$

Finally, shifting the integration variable back, we obtain

$$P_m(y) =$$
$$\int \prod_{i_1<\ldots i_p} P_J(J_{i_1\ldots i_p}) dJ_{i_1\ldots i_p} \, \frac{1}{Z_J(\beta)^2} \sum_{\{\sigma_i\}} \sum_{\{\tau_i\}} \delta\left(y - \tfrac{1}{N}\sum_i \sigma_i\tau_i \right) \exp\left[-\beta\mathcal{H}_p(\{\sigma_i\}) - \beta\mathcal{H}_p(\{\tau_i\}) \right]$$
$$= P_q(y) \tag{46}$$

which completes the proof.

Appendix C.2 Other proofs concerning the Nishimori line

In this subsection, we prove the results concerning the Nishimori line and two triple points mentioned in §5. (The demonstration of several mathematical identities used here is left to Appendix C.3.) We first notice that (25) means not only that the ferromagnet on the Nishimori line ($p\beta J^2 = 2J_0$) is replica symmetric, but that it has $q = M$. It follows that $\frac{1}{2}p\beta^2 J^2 q^{p-1} = \beta J_0 M^{r-1}$, and with (10) this is βh. We may verify $q = M$ independently of the gauge result, as using (15) and (17) this becomes

$$\int \frac{dz}{\sqrt{2\pi}} e^{-z^2/2} \tanh^2\left(\sqrt{\beta h} z + \beta h \right) = \int \frac{dz}{\sqrt{2\pi}} e^{-z^2/2} \tanh\left(\sqrt{\beta h} z + \beta h \right), \tag{47}$$

an identity proved in Appendix C.3.

The spin glass transition line satisfies (20) with $x = 1$ and $q_0 = h = 0$ (as $M = 0$). Matters are simplified by the independence of G from z_0, which means that the integrals over z_0 become trivial. The assertion that the q_1 here is the same as the q of the RS ferromagnet on the Nishimori line becomes, with (20b),

$$\int \frac{dz}{\sqrt{2\pi}} e^{-z^2/2} \tanh^2\left(\sqrt{\beta h} z + \beta h \right) = \frac{\int \frac{dz_1}{\sqrt{2\pi}} e^{-z_1^2/2} \cosh\left(\sqrt{\beta h} z_1 \right) \tanh^2\left(\sqrt{\beta h} z_1 \right)}{\int \frac{dz_1}{\sqrt{2\pi}} e^{-z_1^2/2} \cosh\left(\sqrt{\beta h} z_1 \right)}, \tag{48}$$

which is also proved in Appendix C.3. The other non-trivial self-consistent equation, (20c), becomes

$$\frac{1}{4}(p-1)\beta^2 J^2 q^p = -\ln \int \frac{dz_1}{\sqrt{2\pi}} e^{-z_1^2/2} \cosh\left(\sqrt{\beta h} z_1 \right)$$
$$+ \frac{\int \frac{dz_1}{\sqrt{2\pi}} e^{-z_1^2/2} \cosh\left(\sqrt{\beta h} z_1 \right) \ln\cosh\left(\sqrt{\beta h} z_1 \right)}{\int \frac{dz_1}{\sqrt{2\pi}} e^{-z_1^2/2} \cosh\left(\sqrt{\beta h} z_1 \right)}. \tag{49}$$

The thermodynamic transition line is located by equating the free energy of the ferromagnetic solution and that of the paramagnetic or spin glass solution. The free energy for $r = p$ is related to that in a field via (6) and (8). Where the thermodynamic and spin glass transition lines cross, the free energy of the spin glass is $f_{\rm SG} = f_{\rm field}^{\rm (1RSB)}$ with $x = 1$, $q_0 = h = 0$, and $f_{\rm field}^{\rm (1RSB)}$ given by (18).

If the Nishimori line passes through this point then the previous results apply. The free energy of the ferromagnet is therefore

$$f_{\rm FM} = f_{\rm field}^{\rm (RS)} + hM - \tfrac{1}{r}J_0 M^r = f_{\rm field}^{\rm (RS)} + \tfrac{1}{2}(p-1)\beta J^2 q^p \tag{50}$$

with $f_{\rm field}^{\rm (RS)}$ given by (14). The thermodynamic transition condition $f_{\rm FM} = f_{\rm SG}$ becomes

$$\frac{1}{4}(p-1)\beta^2 J^2 q^p - \int \frac{dz}{\sqrt{2\pi}}\, e^{-z^2/2} \ln\cosh\left(\sqrt{\beta h}z + \beta h\right) = -\ln \int \frac{dz_1}{\sqrt{2\pi}}\, e^{-z_1^2/2} \cosh\left(\sqrt{\beta h}z_1\right) \tag{51}$$

or, using (49),

$$\frac{\int \frac{dz_1}{\sqrt{2\pi}}\, e^{-z_1^2/2} \cosh\left(\sqrt{\beta h}z_1\right) \ln\cosh\left(\sqrt{\beta h}z_1\right)}{\int \frac{dz_1}{\sqrt{2\pi}}\, e^{-z_1^2/2} \cosh\left(\sqrt{\beta h}z_1\right)} - \int \frac{dz}{\sqrt{2\pi}}\, e^{-z^2/2} \ln\cosh\left(\sqrt{\beta h}z + \beta h\right) = 0\,, \tag{52}$$

which is also proved in Appendix C.3. Thus, the Nishimori line does pass through the thermodynamic triple point where the paramagnet, spin glass, and RS ferromagnets meet.

The equations for the intersection of spinodal line and the C1RSB transition line are discussed in Appendix B. If this point lies on the Nishimori line then the above results apply. Setting $p = r$, $M = q$, and $\frac{1}{2}p\beta^2 J^2 q^{p-1} = \beta h$ in (39) and in (16) as an equality, dividing the former by the latter, and dividing the result by $\frac{1}{2}p(p-1)\beta^2 J^2 q^{p-1}$, gives a condition for the consistency of this hypothesis which may be written

$$\int \frac{dz}{\sqrt{2\pi}}\, e^{-z^2/2} \operatorname{sech}^4\left(\sqrt{\beta h}z + \beta h\right) - 1 + \int \frac{dz}{\sqrt{2\pi}}\, e^{-z^2/2} \tanh^2\left(\sqrt{\beta h}z + \beta h\right) + \frac{\left[\int \frac{dz}{\sqrt{2\pi}}\, e^{-z^2/2} \tanh\left(\sqrt{\beta h}z + \beta h\right) \operatorname{sech}^2\left(\sqrt{\beta h}z + \beta h\right)\right]^2}{\int \frac{dz}{\sqrt{2\pi}}\, e^{-z^2/2} \tanh^2\left(\sqrt{\beta h}z + \beta h\right) \operatorname{sech}^2\left(\sqrt{\beta h}z + \beta h\right)} = 0\,, \tag{53}$$

which is proved in Appendix C.3. Thus, the Nishimori line also passes through the spinodal triple point where the paramagnet, RS ferromagnet, and RSB ferromagnet meet.

Appendix C.3 Proofs of some mathematical identities

In this section we prove several identities used in Appendix C.2. These proofs will all rely on the lemmas

$$\int \frac{dz}{\sqrt{2\pi}}\, e^{-z^2/2} \cosh(az) f(z) = e^{a^2/2} \int \frac{dz}{\sqrt{2\pi}}\, e^{-z^2/2} f_{\rm E}(z+a) \tag{54}$$

$$\int \frac{dz}{\sqrt{2\pi}}\, e^{-z^2/2} \sinh(az) f(z) = e^{a^2/2} \int \frac{dz}{\sqrt{2\pi}}\, e^{-z^2/2} f_{\rm O}(z+a) \tag{55}$$

where $f_{\rm E}$ and $f_{\rm O}$ are the even and odd parts of the function f. The proof of these runs as follows:

$$\int \frac{dz}{\sqrt{2\pi}}\, e^{-z^2/2} \left\{ \begin{matrix} \cosh(az) \\ \sinh(az) \end{matrix} \right\} f(z) = \frac{1}{2} \int \frac{dz}{\sqrt{2\pi}}\, e^{-z^2/2} \left(e^{az} \pm e^{-az}\right) f(z) \tag{56}$$

$$= \frac{1}{2} e^{a^2/2} \int \frac{dz}{\sqrt{2\pi}}\, \left(e^{-(z-a)^2/2} \pm e^{-(z+a)^2/2}\right) f(z) \tag{57}$$

$$= \frac{1}{2} e^{a^2/2} \left(\int \frac{dz_1}{\sqrt{2\pi}}\, e^{-z_1^2/2} f(z_1 + a) \pm \int \frac{dz_2}{\sqrt{2\pi}}\, e^{-z_2^2/2} f(-z_2 - a) \right) \tag{58}$$

$$= e^{a^2/2} \int \frac{dz}{\sqrt{2\pi}}\, e^{-z^2/2} \left\{ \begin{matrix} f_{\rm E}(z+a) \\ f_{\rm O}(z+a) \end{matrix} \right\}. \tag{59}$$

The proof of (47) now runs as follows:

$$\int \frac{dz}{\sqrt{2\pi}}\, e^{-z^2/2} \tanh^2(az+a^2) = e^{-a^2/2} \int \frac{dz}{\sqrt{2\pi}}\, e^{-z^2/2} \cosh(az) \tanh^2(az) \qquad \text{using (54)} \tag{60}$$

$$= e^{-a^2/2} \int \frac{dz}{\sqrt{2\pi}}\, e^{-z^2/2} \sinh(az) \tanh(az) \tag{61}$$

$$= \int \frac{dz}{\sqrt{2\pi}}\, e^{-z^2/2} \tanh(az+a^2) \qquad \text{using (55).} \tag{62}$$

The proof of (48) runs as follows:

$$\int \frac{dz}{\sqrt{2\pi}}\, e^{-z^2/2} \cosh(az) = e^{a^2/2} \int \frac{dz}{\sqrt{2\pi}}\, e^{-z^2/2} \qquad \text{using (54)} \tag{63}$$

$$= e^{a^2/2}\,; \tag{64}$$

$$\int \frac{dz}{\sqrt{2\pi}}\, e^{-z^2/2} \cosh(az) \tanh^2(az) = e^{a^2/2} \int \frac{dz}{\sqrt{2\pi}}\, e^{-z^2/2} \tanh^2(az+a^2)\,; \qquad \text{using (54)} \tag{65}$$

$$\frac{\int \frac{dz}{\sqrt{2\pi}}\, e^{-z^2/2} \cosh(az) \tanh^2(az)}{\int \frac{dz}{\sqrt{2\pi}}\, e^{-z^2/2} \cosh(az)} = \int \frac{dz}{\sqrt{2\pi}}\, e^{-z^2/2} \tanh^2(az+a^2)\,, \tag{66}$$

and the proof of (52) is identical with $\tanh^2$ replaced by $\ln\cosh$.

The proof of (53) runs as follows: using (54),

$$\int \frac{dz}{\sqrt{2\pi}}\, e^{-z^2/2} \operatorname{sech}^4(az+a^2) = e^{-a^2/2} \int \frac{dz}{\sqrt{2\pi}}\, e^{-z^2/2} \cosh(az) \operatorname{sech}^4(az)\,, \tag{67}$$

$$1 = e^{-a^2/2} \int \frac{dz}{\sqrt{2\pi}}\, e^{-z^2/2} \cosh(az)\,, \tag{68}$$

$$\int \frac{dz}{\sqrt{2\pi}}\, e^{-z^2/2} \tanh^2(az+a^2) = e^{-a^2/2} \int \frac{dz}{\sqrt{2\pi}}\, e^{-z^2/2} \cosh(az) \tanh^2(az)\,; \tag{69}$$

using (55),

$$\int \frac{dz}{\sqrt{2\pi}}\, e^{-z^2/2} \tanh(az+a^2) \operatorname{sech}^2(az+a^2)$$

$$= e^{-a^2/2} \int \frac{dz}{\sqrt{2\pi}}\, e^{-z^2/2} \sinh(az) \tanh(az) \operatorname{sech}^2(az) \tag{70}$$

$$= e^{-a^2/2} \int \frac{dz}{\sqrt{2\pi}}\, e^{-z^2/2} \cosh(az) \tanh^2(az) \operatorname{sech}^2(az)\,; \tag{71}$$

and using (54) again

$$\int \frac{dz}{\sqrt{2\pi}}\, e^{-z^2/2} \tanh^2(az+a^2) \operatorname{sech}^2(az+a^2)$$

$$= e^{-a^2/2} \int \frac{dz}{\sqrt{2\pi}}\, e^{-z^2/2} \cosh(az) \tanh^2(az) \operatorname{sech}^2(az)\,; \tag{72}$$

thus

$$\int \frac{dz}{\sqrt{2\pi}}\, e^{-z^2/2} \operatorname{sech}^4(az+a^2) - 1 + \int \frac{dz}{\sqrt{2\pi}}\, e^{-z^2/2} \tanh^2(az+a^2)$$

$$+ \frac{\left[\int \frac{dz}{\sqrt{2\pi}}\, e^{-z^2/2} \tanh(az+a^2) \operatorname{sech}^2(az+a^2)\right]^2}{\int \frac{dz}{\sqrt{2\pi}}\, e^{-z^2/2} \tanh^2(az+a^2) \operatorname{sech}^2(az+a^2)}$$

$$= e^{-a^2/2} \int \frac{dz}{\sqrt{2\pi}}\, e^{-z^2/2} \cosh(az) \left[\operatorname{sech}^4(az) - 1 + \tanh^2(az) + \tanh^2(az) \operatorname{sech}^2(az)\right]\,; \tag{73}$$

and this is identically zero since the term in square brackets vanishes using $\operatorname{sech}^2(az) = 1 - \tanh^2(az)$.

Acknowledgments

PG and DS would like to thank EPSRC (UK) for financial support, PG for research studentship 97304251 and DS for research grant GR/M04426. HN acknowledges the support of the Sumitomo Foundation. This work was also supported by the Anglo–Japanese Collaboration Programme between The Royal Society and the Japan Society for the Promotion of Science.

References

[1] M. Mézard, G. Parisi, and M. A. Virasoro, *Spin Glass Theory and Beyond* (World Scientific, 1987).

[2] D. Sherrington, "Spin Glasses", in *Physics of Novel Materials* (World Scientific, 1999), edited by M. P. Das.

[3] J. A. Mydosh, *Spin glasses: an experimental introduction* (Taylor and Francis, 1993).

[4] J. A. Hertz, A. Krogh, and R. G. Palmer, *Introduction to the theory of neural computation* (Addison–Wesley, 1991).

[5] P. G. Wolynes, J. N. Onuchic, and D. Thirumalai, Science **267**, 1619 (1995).

[6] N. Sourlas, Nature **339**, 693 (1989).

[7] E. Gardner, Nucl. Phys. B **257**, 747 (1985).

[8] V. M. de Oliveira and J. F. Fontanari, J. Phys. A **32**, 2285 (1998).

[9] H. Nishimori and K. Y. M. Wong, Phys. Rev. E **60**, 132 (1999).

[10] P. Gillin and D. Sherrington, J. Phys. A **33**, 3081 (2000).

[11] D. Sherrington and S. Kirkpatrick, Phys. Rev. B **17**, 4384 (1978).

[12] G. Parisi, J. Phys. A **13**, 1101 (1979).

[13] B. Derrida, Phys. Rev. B **24**, 2613 (1981).

[14] T. C. Dorlas and J. R. Wedagedera, Phys. Rev. Lett. **83**, 4441 (1999).

[15] J. R. L. de Almeida and D. J. Thouless, J. Phys. A **11**, 983 (1978).

[16] G. Parisi, J. Phys. A **13**, L115 (1979).

[17] H. Nishimori, Prog. Theor. Phys. **66**, 1169 (1981).

[18] P. Gillin and D. Sherrington, to appear in J. Phys. A (2001), `cond-mat/0101245`.